Observation of Interference between Dielectronic Recombination and Radiative Recombination in Highly Charged Uranium Ions

D. A. Knapp, P. Beiersdorfer, M. H. Chen, J. H. Scofield, and D. Schneider

Physics Department, Lawrence Livermore National Laboratory, Livermore, California 94550

(Received 25 October 1993)

We have performed high-resolution measurements of photon excitation functions for radiative recombination and dielectronic recombination in highly charged uranium ions. The data show evidence for quantum interference between the two processes in the vicinity of the *KLL* resonances.

PACS numbers: 34.80.Kw, 32.80.Hd, 52.25.Nr

Radiative recombination, the radiative capture of a free electron by an ion, and dielectronic recombination, a resonant radiative capture process, should, in principle, interfere. This interference should be largest for highly charged high-Z ions, in which the cross sections for the two processes are most nearly equal. However, the magnitude of this effect has been predicted to be too small to observe with present techniques in those high-Z systems for which it has been calculated [1]. In this Letter we present the first observation of the high-energy *KLL* dielectronic recombination resonances in few-electron high-Z ions. In these resonances, we observe significant interference between dielectronic recombination and radiative recombination.

In radiative recombination, illustrated in Fig. 1(a), an electron is captured into a bound state of an ion, emitting a photon with an energy equal to the initial energy of the electron plus the binding energy of the state into which it is captured. In dielectronic recombination, illustrated in Fig. 1(b), a free electron is captured into a vacant bound state via an inverse Auger process, while a previously bound electron is excited. If the resulting intermediate doubly excited state decays radiatively, the process is known as dielectronic recombination. To be resonant, the initial energy of the free electron plus the binding energy of the state to which it is captured must equal the energy difference between the ground state and the excited state of the bound electron.

Dielectronic recombination resonances are labeled by the principal quantum numbers of the electrons that form the excited intermediate state; thus, the *KLL* dielectronic recombination resonances are those in which an electron is captured into the L shell, while another electron is excited from the K shell to the L shell. In high-Z ions, the L shell splits into two distinct subshells: the L_{12} shell, which contains the $2s_{1/2}$ and $2p_{1/2}$ levels, and the L_3 shell, which contains the $2p_{3/2}$ states. This splitting gives rise to three groupings of *KLL* dielectronic recombination resonances: the $KL_{12}L_{12}$, $KL_{12}L_3$, and KL_3L_3 resonances.

Dielectronic recombination has been measured extensively in low- and medium-Z ions [2–10], and low-energy ($E_e < 1$ keV) resonances have also been studied in higher-Z ions [5,11]. In general, agreement with theory has been good, especially for dielectronic recombination resonances involving high electron energies. Radiative transfer and excitation, a process similar to dielectronic recombination, but occurring in ion-atom collisions, has been measured for heliumlike and lithiumlike uranium ions [12,13]. These measurements generally agree with theory; however, their resolution is limited by the momentum distribution of electrons in the target atom.

Measurements of high-energy $\Delta n \geq 1$ dielectronic recombination in high-Z ions promise to be sensitive to

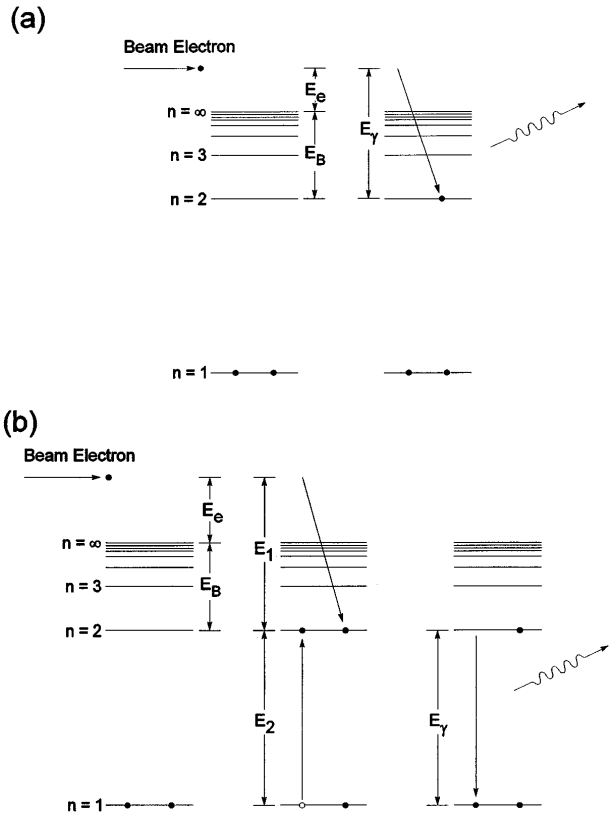

FIG. 1. (a) Illustration of radiative recombination. An electron is captured into a vacant atomic state with binding energy E_B, emitting a photon with energy $E_\gamma = E_e + E_B$. (b) Illustration of dielectronic recombination. An electron with energy E_e is nonradiatively captured into an excited intermediate state, which then decays radiatively. The resonance condition, $E_1 = E_2$, must be met for this process to occur.

 0031-9007/95/74(1)/54(4)$06.00

relativistic effects, QED effects, and quantum interference between dielectronic recombination and radiative recombination [1,14].

Because of the resonance condition for dielectronic recombination, the emitted photon energy can be nearly identical to that emitted by radiative recombination. In this case, the two processes have the same initial and final states and may therefore interfere. Badnell and Pindzola have calculated the size of this effect in heliumlike U^{90+} ions [1], extending the theoretical framework of Jacobs, Cooper, and Haan [15]. They point out that for high-Z ions, it is possible for the dielectronic recombination and radiative recombination cross sections to be comparable, enhancing the possibility of interference. Based upon calculations of the total recombination cross sections, they concluded that the effect would be too small to observe.

We produced and trapped uranium ions with ionization states from neonlike (U^{82+}) to heliumlike (U^{90+}) in the high-energy Electron Beam Ion Trap (Super-EBIT) at the Lawrence Livermore National Laboratory. This device creates low energy highly charged ions by sequential ionization in a high-current-density electron beam, which also serves to trap and excite the ions [16]. Photons emitted from electron-ion interactions were detected at 90° to the electron beam direction by two solid-state Ge detectors.

As in our earlier measurements of dielectronic recombination [10], we ramped the electron beam energy over the range of interest while recording the photon energy, beam energy, and time for each observed photon. This technique allows the investigation of dielectronic recombination and radiative recombination over a wide range of electron beam energies while preserving a stable ionization balance.

A false-color scatter plot of typical data is shown in Fig. 2. Radiative recombination photons, whose energy varies with the electron beam energy, are visible as angled bands, and dielectronic recombination photons appear as bright spots, most of which are superimposed on the radiative recombination bands. The three resonance manifolds are well separated from each other, located at electron energies of about 63, 67.5, and 72 keV. In most dielectronic recombination experiments, the process has been measured by observing the total number of recombination events as a function of electron energy. In the present experiment, by contrast, we monitor the photon associated with the recombination event. This technique allows the selection of specific final states for the recombination process. Recombination events for capture into a specific subshell can be projected onto the electron beam energy axis to give excitation functions. The raw data for such excitation functions for events along the L_{12}, L_3, and M radiative recombination lines are shown in Fig. 3. The total recombination rate for these three channels at a particular electron energy is more than an order of magnitude larger than the rate for the L_{12} channel alone. By selecting only the events in the L_{12} cut we greatly enhance our sensitivity to interference.

The selection of events from the L_{12} radiative recombination band also allows a simplified analysis. The ions in the trap are all in the ground state (with the exception of berylliumlike ions in the $1s^2 2s 2p\ ^3P_0$ metastable state, which has a nearly infinite lifetime). Only those ions with a hole in the L_{12} subshells (i.e., ionization states from boronlike through heliumlike) can experience radiative recombination to the selected states. Similarly, the observed dielectronic recombination resonance manifolds can only appear for a limited number of ionization states; the $KL_{12}L_{12}$ resonances are only accessible to ionization states from berylliumlike through heliumlike, while the $KL_{12}L_3$ are accessible to boronlike through heliumlike ions. Thus, the analysis of these events need only include four ionization states.

Interference between dielectronic recombination and radiative recombination will produce asymmetric resonance line shapes characterized by a Fano profile [17,18] for the

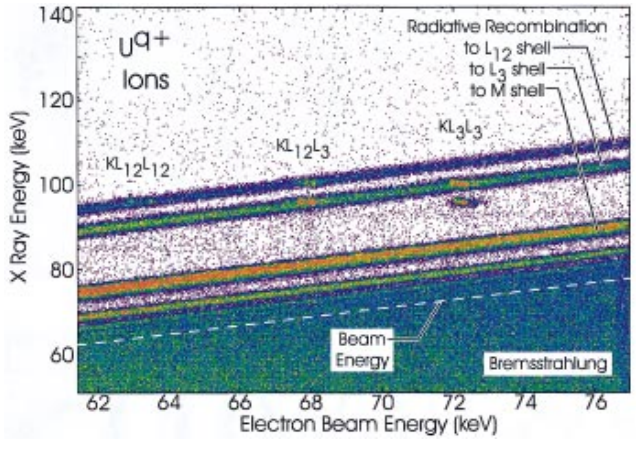

FIG. 2. False-color scatter plot of raw data. The angled bands are radiative recombination photons, whose energy increases with increasing beam energy. The bright spots are photons from dielectronic recombination resonances.

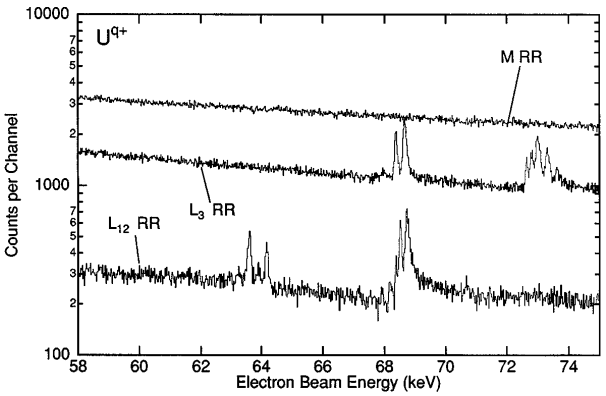

FIG. 3. Projection of recombination events from the L_{12}, L_3, and M radiative recombination bands onto the electron beam energy axis.

combined processes. As can be see in Fig. 3, the $KL_{12}L_3$ resonance manifold exhibits a marked asymmetry, with a long tail on the high-energy side and a relative decrease in the radiative recombination rate between the $KL_{12}L_{12}$ and $KL_{12}L_3$ resonance manifolds.

Our analysis precludes the possibility that the observed effect is an instrumental artifact. The shape of the electron beam-energy distribution was measured using the photons from KL_3L_3 resonances that do not coincide with any radiative recombination photons. It is a symmetric Gaussian. During data acquisition, the electron beam energy was scanned through the resonances in both directions, from high energy to low energy and vice versa. The observed resonance shapes from the different directions are identical; thus, they cannot be the result of ionization-balance changes induced as the beam energy passed through the resonances. The excitation function for radiative recombination to the $n = 3$ shell was measured over the entire energy range. It is completely smooth, eliminating the possibility of any structure in the ion-beam overlap. Finally, the resonances were recorded with two separate scans over different energy ranges. Any differences might be attributed to problems in the data-acquisition electronics; none were observed.

To analyze the data, the theoretical dielectronic recombination resonance strengths, resonance energies, and widths were calculated using a multiconfiguration Dirac-Fock model [19,20], and radiative recombination cross sections were computed using Dirac-Slater wave functions [21,22]. The data from the L_{12} radiative recombination band were then fit to Lorentzian and Fano profiles. For these fits, the dielectronic recombination resonance energies and widths are fixed, as are the relative resonance strengths within each ionization state. The peak profiles are convoluted with a Gaussian beam-energy distribution and added to the radiative recombination amplitude. The ionization balance is not known *a priori* and is therefore fitted, as described in our earlier results [10], as is an overall scaling factor for the dielectronic recombination resonance strengths relative to the radiative recombination cross section.

The fit of the $KL_{12}L_3$ resonances using Lorentzian line shapes is shown in Fig. 4(a). The deficit on the low-energy side and excess on the high-energy side of the manifold are both clearly visible in the residuals, shown in Fig. 4(b).

The Fano profile used to fit the resonances is given by [17,18]

$$\sigma(E) = \sigma_a \frac{(q + \epsilon)^2}{1 + \epsilon^2} + \sigma_b, \qquad (1)$$

where $\epsilon = (E - E_0)/(\Gamma/2)$, σ_a and σ_b are the interfering and noninterfering parts of the continuum cross section, respectively, and q is the Fano line-shape factor. Small q values imply large interference. The heliumlike and lithiumlike ionization states have a number of small, overlapping resonances; no attempt was made to fit the

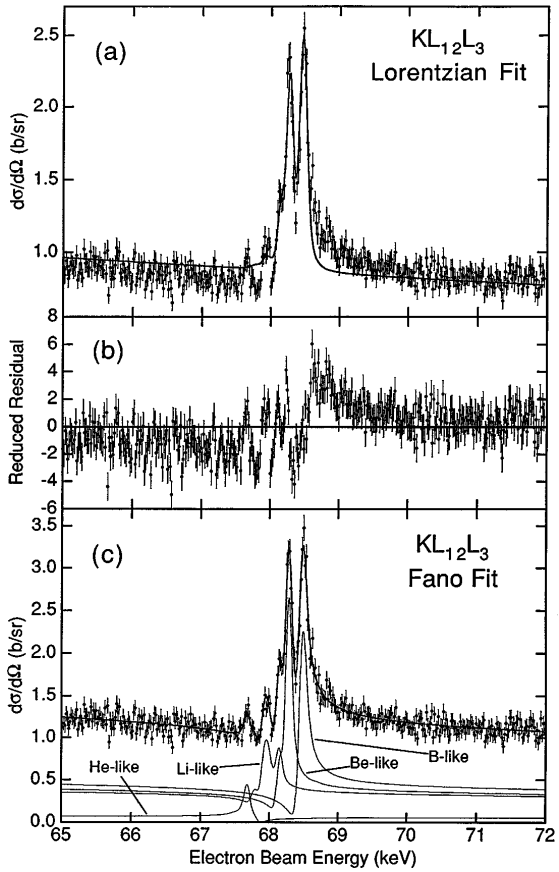

FIG. 4. (a) Fit of $KL_{12}L_3$ resonance data with a non-Fano line shape. The resonance energies, relative resonance intensities within each ionization state, and resonance widths are all fixed to theoretical predictions from Ref. [19]. The χ^2 value for this fit is 1092.7 for 367 degrees of freedom. (b) Reduced residuals for this fit. (c) Fit of $KL_{12}L_3$ resonance data with a Fano line shape. The same parameters were fixed as those in the non-Fano fit. The χ^2 value for this fit is 369.5 for 364 degrees of freedom.

Fano line-shape factor for each one. Instead, a single q was used for all the resonances of each ionization state. This approximation is justified because the berylliumlike and boronlike ionization states dominate the ionization balance, and each only has one strong resonance in this energy region. The fit is shown in Fig. 4(c). Despite the simplicity of the assumptions used, the agreement with the data is striking.

Interference was also observed in the $KL_{12}L_{12}$ resonances, though the magnitude of the effect is much smaller. The resulting sign of the q parameters is reversed from that deduced for the $KL_{12}L_3$ resonances.

We present the fitted q values from the $KL_{12}L_3$ manifold for each ionization state in Table I. Since the berylliumlike and boronlike ionization states dominate the ionization balance, and each has only one large resonance in this manifold, their q values can be determined reliably. In contrast, the data do not allow firm conclusions to be drawn about the physical significance of the fit-

TABLE I. Parameters from Fano fit of $KL_{12}L_3$ resonances. Errors are statistical only. Minimum q values are for the strongest resonance for each ionization state.

Ionization state	Relative population	Fitted q	Strongest $q_{\min}$
Heliumlike	1.3%	−3.2(7)	7.8
Lithiumlike	11.1%	4.0(6)	6.1
Berylliumlike	26.3%	4.8(4)	4.4
Boronlike	61.3%	2.9(2)	2.8

ted q values for the heliumlike and lithiumlike ionization states. Since each has several contributing resonances in this manifold whose relative resonance strengths were fixed in the fit, the fitted Fano profiles for these ionization states may result from the fitting algorithm's attempt to compensate for different relative resonance strengths within each ionization state predicted rather than reflecting a true Fano line shape.

A simple test to establish whether the fitted q values are reasonable can be performed by assuming maximum interference; that is, setting $\sigma_b = 0$. In this case, a minimum value for q can be obtained:

$$q_{\min} = \sqrt{\frac{\sigma_{DR}(E_0)}{\sigma_a(E_0)}}. \quad (2)$$

In Table I, we include the value of $q_{\min}$ for the strongest resonance in each ionization state. For the berylliumlike and boronlike ionization states, with single strong resonances, the agreement is good, indicating nearly maximum interference.

The technique of recording the photon energy and electron beam energy for every observed event has resulted in the first observation of interference between radiative recombination and dielectronic recombination. The influence of this interference on the L_{12} radiative recombination cross section in the vicinity of the KLL resonances of uranium ions is significant for electron energies up to 2.5 keV above and below the central resonances.

This research was performed under the auspices of the U.S. Department of Energy at the Lawrence Livermore National Laboratory under Contract No. W-7405-ENG-48. We would especially like to thank J. Martinez, of the DOE Office of Basic Energy Sciences, for his support of this program.

[1] N. R. Badnell and M. S. Pindzola, Phys. Rev. A **45**, 2820 (1992).
[2] P. F. Dittner and S. Datz, in *Recombination of Atomic Ions*, edited by W. G. Graham *et al.*, NATO ASI Ser. B, Vol. 296 (Plenum Press, New York, 1992), p. 133.
[3] L. H. Andersen, in (Ref. [2]), p. 143.
[4] G. Kilgus *et al.*, Phys. Rev. A **46**, 5730 (1992); G. Kilgus *et al.*, Phys. Rev. A **47**, 4859 (1993).
[5] A. Müller, in (Ref. [2]), p. 155.
[6] D. R. DeWitt *et al.*, Phys. Rev. Lett. **68**, 1694 (1992); D. R. DeWitt *et al.*, Phys. Rev. A **44**, 7185 (1991).
[7] M. B. Schneider *et al.*, Phys. Rev. A **45**, R1291 (1992).
[8] R. Ali *et al.*, Phys. Rev. A **44**, 223 (1991); R. Ali *et al.*, Phys. Rev. Lett. **64**, 633 (1990).
[9] P. Beiersdorfer *et al.*, Phys. Rev. A **46**, 3812 (1992); P. Beiersdorfer *et al.*, Rev. Sci. Instrum. **63**, 5029 (1992).
[10] D. A. Knapp *et al.*, Phys. Rev. A **47**, 2039 (1993).
[11] W. Spies *et al.*, Phys. Rev. Lett. **69**, 2768 (1992).
[12] W. G. Graham *et al.*, Phys. Rev. Lett. **65**, 2773 (1990).
[13] J. A. Tanis *et al.*, Nucl. Instrum. Methods Phys. Res., Sect. B **53**, 442 (1991).
[14] P. Zimmerer, N. Grün, and W. Scheid, Phys. Lett. **A 148**, 457 (1990); P. Zimmerer *et al.*, in *Proceeding of the XVIII International Conference on the Physics of Electronic and Atomic Collisions—Abstracts of Contributed Papers*, edited by T. Andersen, B. Fastrup, F. Folkmann, and H. Knudsen, (AIP, New York, 1993), Vol. I, p. 380.
[15] V. L. Jacobs, J. Cooper, and S. L. Haan, Phys. Rev. A **36**, 1093 (1987).
[16] D. A. Knapp *et al.*, Nucl. Instrum. Methods Phys. Res., Sect. A **334**, 305 (1993).
[17] U. Fano, Phys. Rev. **124**, 1866 (1961).
[18] U. Fano and J. W. Cooper, Phys. Rev. **137**, A1364 (1965).
[19] M. H. Chen, Phys. Rev. A **45**, 4604 (1992).
[20] M. H. Chen (unpublished).
[21] J. Scofield, Phys. Rev. A **40**, 3054 (1989).
[22] J. Scofield (unpublished).